Optical Materials: X 22 (2024) 100305

Contents lists available at ScienceDirect

Optical Materials: X

journal homepage: www.journals.elsevier.com/optical-materials-x

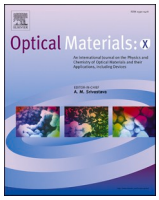

Effect of Ga^{3+}/Sc^{3+} on Yb^{3+} emission in mixed YAG at cryogenic temperatures

Jan Hostaša [a,*], Venkatesan Jambunathan [b], Dariia Chernomorets [a,c], Andreana Piancastelli [a], Chiara Zanelli [a], Great Chayran [b], Francesco Picelli [a], Martin Smrž [b], Valentina Biasini [a], Tomáš Mocek [b], Laura Esposito [a]

[a] CNR ISSMC - Institute of Science, Technology and Sustainability for Ceramics (former ISTEC), Via Granarolo 64, 48018, Faenza, (RA), Italy
[b] HiLASE Centre, Institute of Physics of the Czech Academy of Sciences, V.v.i., Za Radnicí 828, 25241, Dolní Břežany, Czech Republic
[c] Institute for Single Crystals of NAS of Ukraine, 60 Nauky Ave., Kharkiv, 61072, Ukraine

ARTICLE INFO

Keywords:
Mixed garnets
Emission
Ceramics
Cryogenics

ABSTRACT

We studied the effect of $Ga^{3+}$and Sc^{3+} on Yb:YAG emission at cryogenic temperatures on three different mixed garnets namely Yb:YGAG, Yb:YSAG and Yb:YSGAG. The compositional tuning of these mixed garnets was achieved by preparing ceramic pellets by solid state reaction with different concentration of Ga^{3+}, or Sc^{3+}, or both. The incorporation of Sc^{3+} in Yb:YAG leads only to a limited spectral broadening. On the other hand, the incorporation of either Ga^{3+} or both Ga^{3+} and Sc^{3+} results in a significant spectral broadening. In the latter case, this inhomogeneous broadening is attributed to the mixed occupancy of both Ga^{3+} and Sc^{3+} in octahedral and tetragonal sites in the crystal lattice leading to a significant distortion in the structure.

1. Introduction

In recent years, the development of high average and peak power (HAPP) lasers has received tremendous interest due to the potential applications such as laser driven inertial fusion [1], high harmonic generation [2], soft x-ray source via laser Compton scattering [3], laser shock peening [4] and others. To develop a HAPP laser system [5,6], proper gain media with excellent material properties are required. In this aspect, Yb:YAG has been studied as an important IR laser gain medium and is currently used in high-energy pulsed lasers, e.g. DiPOLE [7], where large ceramic Yb:YAG slabs are operated under cryogenic cooling. At cryogenic temperatures, Yb:YAG behaves as four-level system with reduced reabsorption losses and exhibits excellent thermo-optical and spectroscopic properties, which play a major role in overall performance of the laser systems [8,9]. Nevertheless, the emission bandwidth of Yb:YAG decreases with decrease in temperature [10,11], that limits the generation of short pulses in the sub picosecond and femtosecond regime which is essential for HAPP laser development. To improve this emission broadening, one way is to introduce some imperfections in the host matrix and create structural irregularities. This approach may be pursued through a modification of the host structure by the substitution of cations. Both Y^{3+} and Al^{3+} ions may be readily substituted by a variety of other ions without compromising the cubic crystalline structure of the material. Typical substituents for the Y^{3+} ions are trivalent ions of lanthanides, for a variety of applications in photonics, which have a similar ionic radius and can be equally coordinated. Yb^{3+} ions are one of the typical examples. Al^{3+}, on the other hand, can be substituted by ions of a similar size such as Sc^{3+} or Ga^{3+}.

To date, emission broadening of mixed garnets doped with several rare earth ions such as Yb, Nd etc. And different cations such as Ga, Sc, Lu, Gd has been studied mainly at room temperature [12–14]. The most studied systems are that of Lu-YAG and Sc-YAG (usually denoted as LuYAG and YSAG, respectively). For LuYAG there are studies on the change in material properties with dopant content [15], room temperature spectroscopic analysis [16], and recently a cryogenic spectroscopic analysis [17] for Yb doping, or a study of Tm-doped system [18]. YSAG was studied for example in Refs. [13,19]. Concerning the emission broadening at cryogenic temperatures, there are only few works from our previous study [20,21]. In one of these, we studied the substitution in the host of 3 at.% Yb:YAG with Gd^{3+} substituting Y^{3+} and Ga^{3+} substituting Al^{3+}. Interesting results were obtained in Ga^{3+} substituted YAG, viz. A significant broadening of the emission spectrum at low temperatures. In the case of Gd^{3+} substitution, the effect was minor. This is in line with the observations of Feng et al. [22]. To further understand

* Corresponding author.
E-mail address: jan.hostasa@issmc.cnr.it (J. Hostaša).

https://doi.org/10.1016/j.omx.2024.100305
Received 15 December 2023; Received in revised form 20 February 2024; Accepted 29 February 2024
Available online 8 March 2024

Table 1
Ionic radii of selected ions depending on the coordination number as reported by Shannon et al. [23].

Ion	Y^{3+}	Yb^{3+}	Gd^{3+}	Al^{3+}	Al^{3+}	Sc^{3+}	Sc^{3+}	Ga^{3+}	Ga^{3+}
Coordination number	8	8	8	4	6	6	8	4	6
Ionic radius	1.019	0.985	1.053	0.39	0.535	0.745	0.87	0.47	0.62

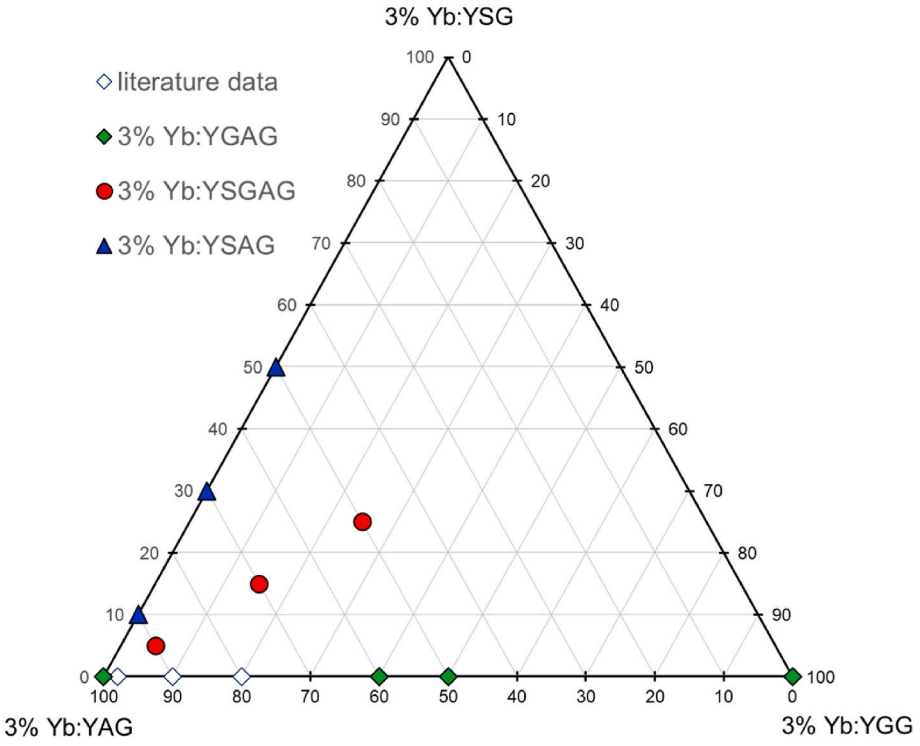

Fig. 1. Ternary diagram showing the compositions of the studied mixed garnets (green points for Ga^{3+} substitution, blue for Sc^{3+} substitution, red for mixed Ga^{3+}, Sc^{3+} substitution and white for data published in Ref. [21]). (For interpretation of the references to colour in this figure legend, the reader is referred to the Web version of this article.)

Table 2
Compositions of the studied mixed garnets; for simplicity, the 3% Yb doping is not mentioned in the mixture and sample names.

Mixture name	Chemical formula
Yb:YAG	$Yb_{0.09}Y_{2.91}Al_5O_{12}$
Yb:YGAG (0.4)	$Yb_{0.09}Y_{2.91}(Al_{0.6}Ga_{0.4})_5O_{12}$
Yb:YGAG (0.5)	$Yb_{0.09}Y_{2.91}(Al_{0.5}Ga_{0.5})_5O_{12}$
Yb:YGG	$Yb_{0.09}Y_{2.91}Ga_5O_{12}$
Yb:YSAG (0.1)	$Yb_{0.09}Y_{2.91}(Al_{0.9}Sc_{0.1})_5O_{12}$
Yb:YSAG (0.3)	$Yb_{0.09}Y_{2.91}(Al_{0.7}Sc_{0.3})_5O_{12}$
Yb:YSAG (0.5)	$Yb_{0.09}Y_{2.91}(Al_{0.5}Sc_{0.5})_5O_{12}$
Yb:YSGAG (0.05,0.05)	$Yb_{0.09}Y_{2.91}(Al_{0.9}Ga_{0.05}Sc_{0.05})_5O_{12}$
Yb:YSGAG (0.15,0.15)	$Yb_{0.09}Y_{2.91}(Al_{0.7}Ga_{0.15}Sc_{0.15})_5O_{12}$
Yb:YSGAG (0.25,0.25)	$Yb_{0.09}Y_{2.91}(Al_{0.5}Ga_{0.25}Sc_{0.25})_5O_{12}$

the effect of concentration on emission broadening we extend our previous work [21] by incorporating different content of Ga^{3+} and Sc^{3+} in the YAG structure. In the present work, we report the results obtained with three systems, characterized in terms of structure and cryogenic emission spectroscopy.

2. Experimental

2.1. Preparation of samples

The compositional tuning of three types of systems was studied. They are.

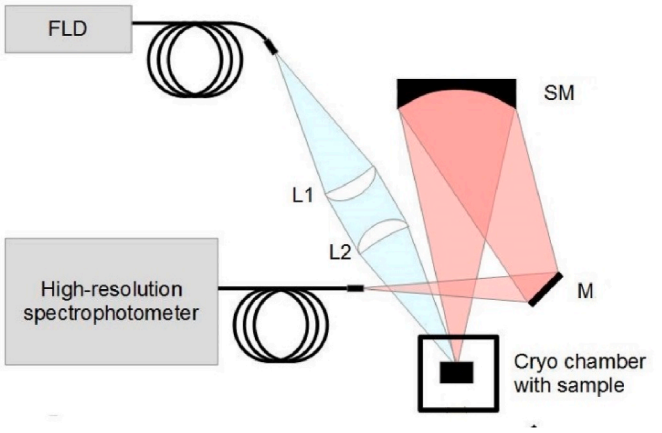

Fig. 2. Cryogenic emission measurement setup. L1, L2 – Achromatic lens. M Silver mirror, SM – spherical mirror. FLD – Fiber coupled laser diode centered at 940 nm, High resolution spectrophotometer.

1. Substitution with Ga^{3+} - hereafter referred as Yb:YGAG system;
2. Substitution with Sc^{3+} - hereafter referred as Yb:YSAG system;
3. Substitution with both Ga^{3+} and Sc^{3+} - hereafter referred as Yb: YSGAG system.

Table 1 lists the ionic radii of the ions relevant to the presented work

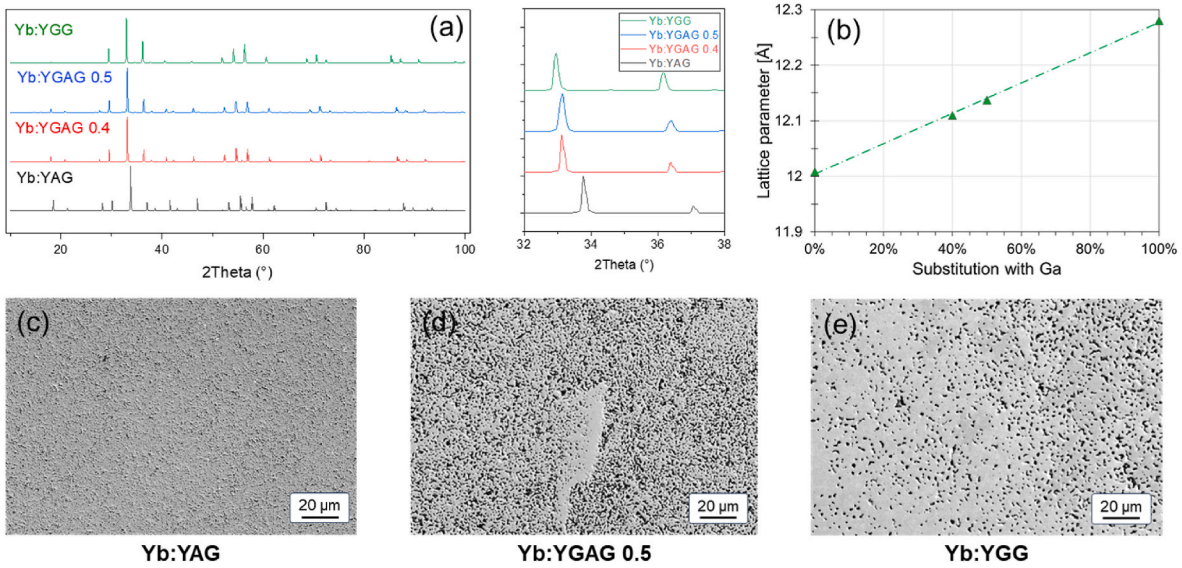

Fig. 3. X-ray diffractograms of compositions with Ga substitution (a) and the lattice parameter plotted in dependence on the substitution of Al^{3+} with Ga^{3+} (b), data points (green triangles) and a linear fit. And SEM picture of a polished sample of Yb:YAG (c), 50% Ga substituted Yb:YAG (d) and Yb:YGG (e). (For interpretation of the references to colour in this figure legend, the reader is referred to the Web version of this article.)

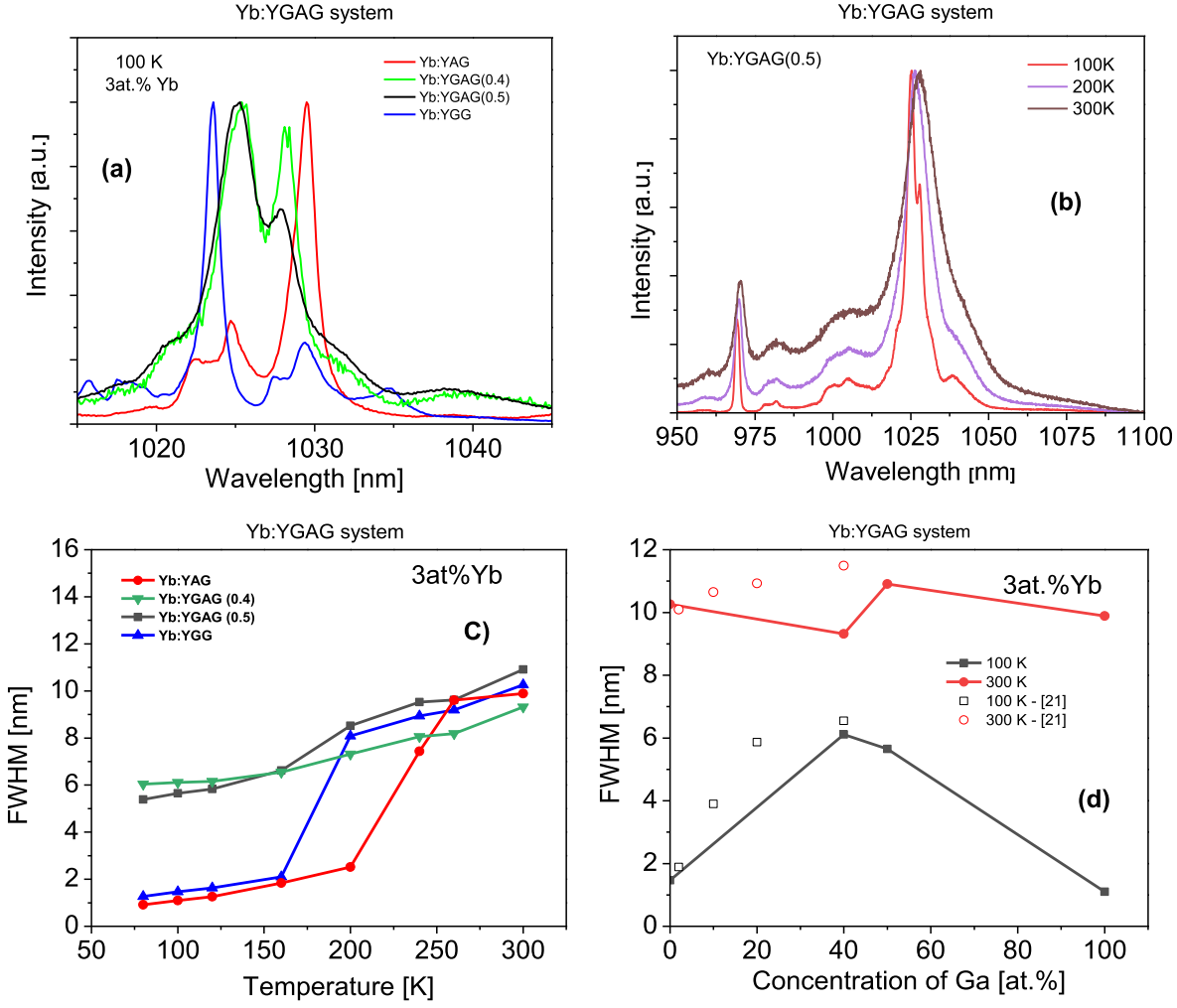

Fig. 4. Emission spectrum measured at 100 K for Yb:YGAG system (a), emission spectra for sample with 50% Ga for 100, 200 and 300 K (b), emission bandwidth (FWHM) at 1030 nm for various temperatures for Yb:YGAG system (c), emission bandwidth (FWHM) at 1030 nm for different Ga content for 100 and 300 K including data from [21] for comparison (d).

Table 3
Emission bandwidth around 1030 nm for the Yb:YGAG systems for various temperatures.

	Emission bandwidth [nm] for the Yb:YGAG system			
Temperature [K]	Yb:YAG	Yb:YGAG (0.4)	Yb:YGAG (0.5)	Yb:YGG
80	1.27	6.04	5.39	0.91
100	1.47	6.11	5.65	1.10
120	1.63	6.16	5.83	1.26
160	2.10	6.55	6.62	1.84
200	8.09	7.32	8.52	2.52
240	8.94	8.06	9.53	7.43
260	9.19	8.19	9.62	9.61
300	10.26	9.32	10.91	9.89

with respect to their coordination in the garnet.

The selected compositions are shown in Fig. 1, along with those studied by Paul David et al. [21].

The general formula is $Yb_{0.09}Y_{2.91}(Al_{1-x-y}Ga_xSc_y)_5O_{12}$ with x and y representing the fraction of Al^{3+} ions substituted by Ga^{3+} and Sc^{3+} ions, respectively. The prepared compositions are listed in Table 2. The naming of the compositions follows the atomic percentage of substitution of Al^{3+} ions by Ga^{3+} or Sc^{3+} ions.

The following high-purity powders were used: Al_2O_3 (≥99.99%, submicrometric, Baikowski, France), Y_2O_3 (≥99.99%, submicrometric, Nippon Yttrium Co., Japan), Yb_2O_3 (≥99.99%, submicrometric, Nippon Yttrium Co., Japan), Ga_2O_3 (≥99.99%, micrometric, Pi-Kem, UK), Sc_2O_3 (≥99.99%, micrometric, Auer Remy, Germany). The powders were mixed for 70 h by ball milling with high-purity Al_2O_3 milling media in absolute ethanol in a polyethylene jar, dried in a dryer at 80 °C and sieved; this process provided a homogeneous mixture of the powders. The obtained powder mixtures were then uniaxially pressed into pellets 15 mm in diameter and treated in air for 1 h at 800 °C in order to remove any organic residues. The samples were sintered in air at 1550 °C with a soaking time of 6 h. The sintered samples were then polished with diamond pastes from 15 μm to 0.25 μm for further characterization.

2.2. Characterization of samples

The samples were subjected to X-ray diffraction studies to determine the structure using Bruker D8 Advance with CuKα source. From the obtained diffraction pattern, the lattice parameters were retrieved using the Rietveld refinement method. To understand the densification of the sintered samples, polished surfaces of the samples were analysed by SEM (ZEISS FEG-SEM Sigma). The cryogenic emission was carried out for all the samples by mounting them in a copper holder. To excite the samples, a fibre coupled diode laser centered at 940 nm was used. To cool the samples a closed-cycle helium cryostat from Cryodyne (Model no: 22C) under vacuum environment to avoid condensation was used. To regulate and monitor the temperature, a 50 Ω resistor and a temperature controller (Lake Shore Cryotronics Inc.) with two silicon diode sensors were used. To collect the emission spectra a photomultiplier tube from Hamamatsu (Model no: H10330A- 25) was used, covering the spectral region 950–1200 nm, and high-resolution spectra were measured using a spectrophotometer from Horiba Jobin Yvon (model no: 1250 M) which has a spectral resolution of 15 p.m. The cryogenic emission measurement setup is illustrated in Fig. 2.

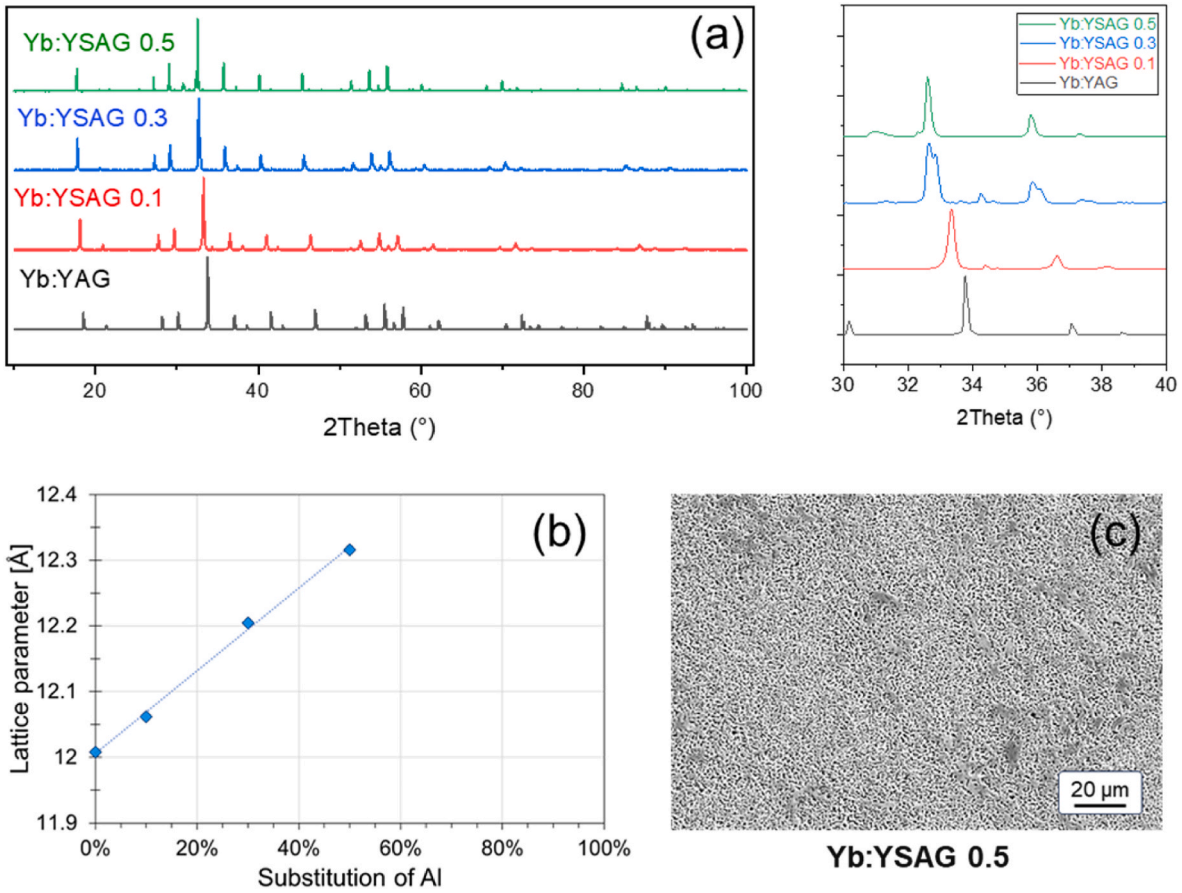

Fig. 5. X-ray diffractograms of compositions with Sc substitution (a) and the lattice parameter plotted in dependence on the substitution with Sc^{3+} (b), data points (green triangles) and a linear fit, (c) SEM picture of 50% Sc substituted Yb:YSAG. (For interpretation of the references to colour in this figure legend, the reader is referred to the Web version of this article.)

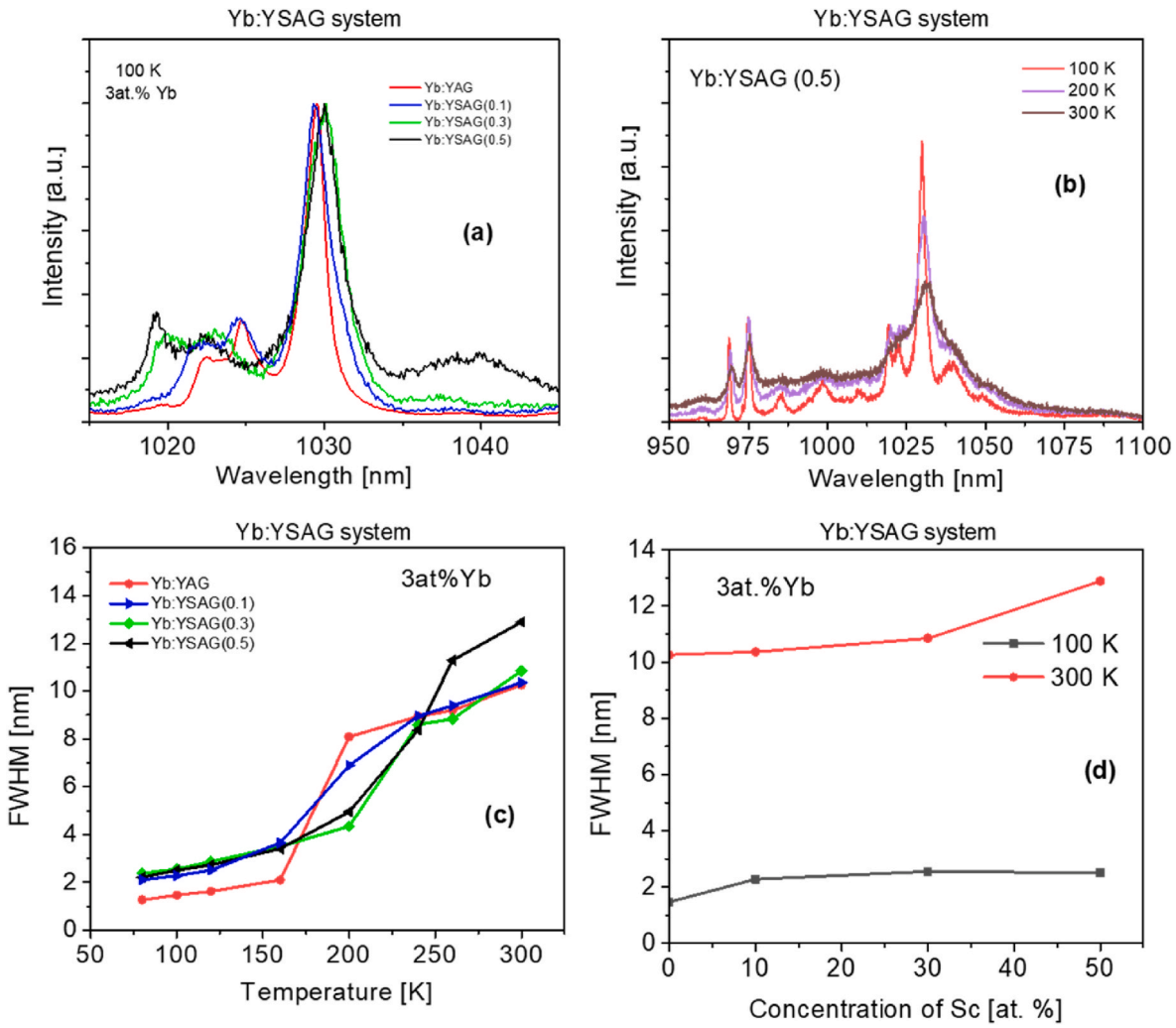

Fig. 6. Emission spectrum measured at 100 K for Yb:YSAG system (a), emission spectra for sample with 50% Sc for 100, 200 and 300 K (b), emission bandwidth (FWHM) at t 1030 nm measured for various temperatures for Yb:YSAG system(c), emission bandwidth (FWHM) at 1030 nm for different Sc content for 100 and 300 K (d).

Table 4
Emission bandwidth around 1030 nm for the Yb:YSAG system for various temperatures.

	Emission bandwidth [nm] for the Yb:YSAG system			
Temperature [K]	Yb:YAG	Yb:YSAG (0.1)	Yb:YSAG (0.3)	Yb:YSAG (0.5)
80	1.27	2.10	2.39	2.22
100	1.47	2.28	2.55	2.51
120	1.63	2.52	2.88	2.73
160	2.10	3.66	3.50	3.42
200	8.09	6.89	4.35	4.95
240	8.94	8.95	8.60	8.37
260	9.19	9.39	8.82	11.29
300	10.26	10.36	10.85	12.89

3. Results and discussion

All the fabricated samples were characterized in terms of structure and cryogenic emission spectroscopy and the results of each system are summarized below. Note that in all the cases of mixed samples the emission peak shifts to a shorter wavelength due to the decrease in crystal field strength which occurs mainly due to the difference on ionic radii between the replacing ion (Al^{3+}) and the replaced ion (Ga^{3+} and/or Sc^{3+}).

3.1. Yb:YGAG system

Fig. 3 a) shows the XRD patterns of the Yb:YGAG system with increasing Ga concentration (Ga substitution of 0, 40%, 50% and 100%). The corresponding chemical formulas are reported in Table 2. The XRD patterns show the presence of a single cubic garnet phase. It can be observed that the diffraction peaks shift towards lower diffraction angle with the increase of Ga content. This corresponds to the increase of the lattice parameter, in line with the larger size of Ga^{3+} ions in comparison to Al^{3+} (see Table 1). The retrieved lattice parameter exhibits a linear increase (see Fig. 3 b). Sintering was performed in air at 1550 °C and did not lead to a full densification of the ceramics. The SEM analysis showed that the addition of Ga leads to microstructural changes. The introduction of Ga leads to a denser microstructure (increase of relative density from about 66% of Yb:YAG to 70% of Yb:YGAG 0.5 and 93% of fully substituted Yb:YGG) and to an enhanced growth of pore size (pores are visible as dark spots in the SEM image). The latter are more visible in the fully substituted Yb:YGG (Fig. 3 e). Emission measurements were carried out in the temperature range from 80 K to 300 K in step size of 40 K (see Fig. 4). For the sake of clarity only few temperatures are shown. Fig. 4 a) shows the emission spectra of a 3 at. % Yb: YGAG system measured around 1030 nm at 100 K. From the figure, we can infer that the substitution of Ga helps in improving the bandwidth even at cryogenic temperatures. Fig. 4b shows the significant narrowing of emission

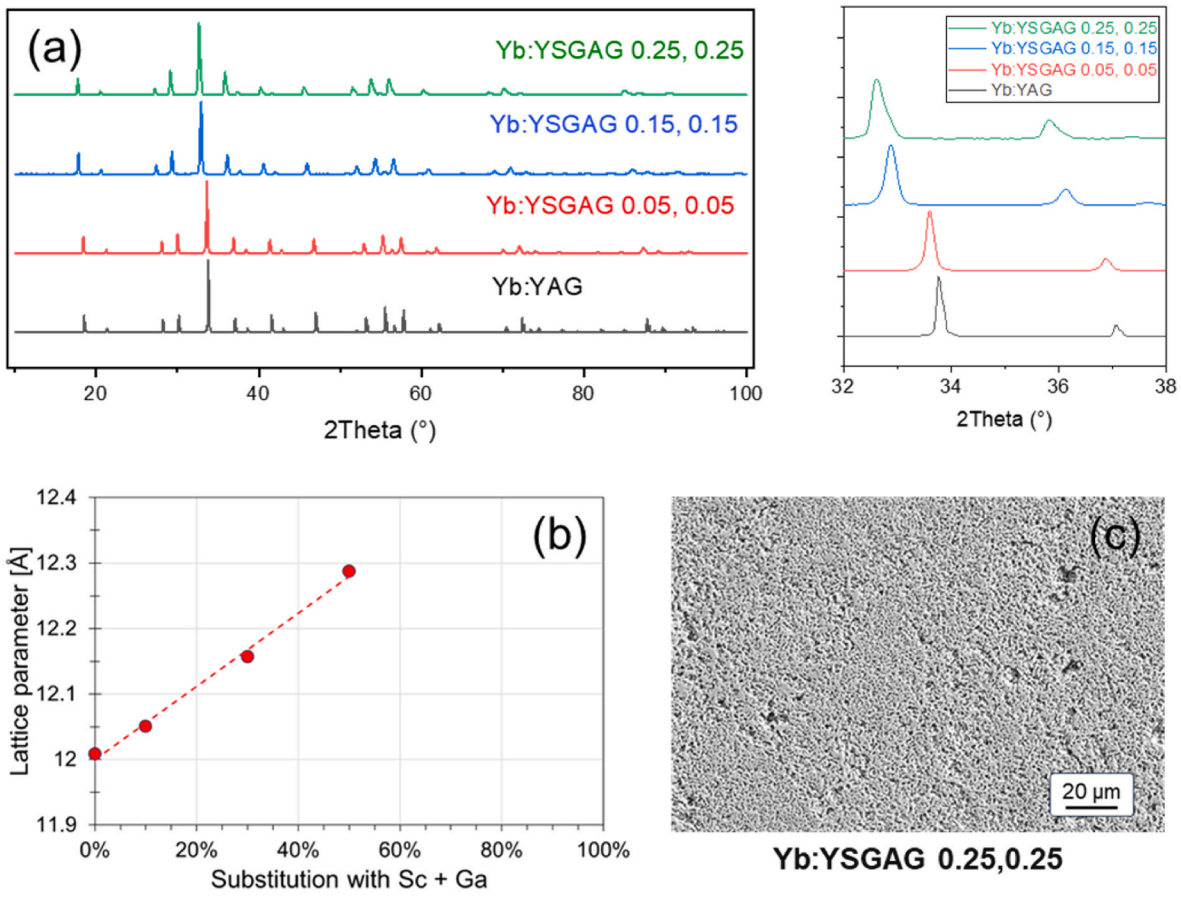

Fig. 7. X-ray diffractograms of compositions with a mixed Ga and Sc substitution (a) and the lattice parameter plotted in dependence on the substitution with Sc^{3+} and Ga^{3+} (b), data points (red circles triangles) and a linear fit, and a SEM image of a 25% Sc and 25% Ga substituted Yb:YSGAG (c). (For interpretation of the references to colour in this figure legend, the reader is referred to the Web version of this article.)

spectra of 50% Ga substitution when the sample is cooled down from 300 K to 100 K. To estimate the variation of emission bandwidth by substitution of Ga, we fitted the gaussian function and the resulting full width half maximum (here after – FWHM) are shown in Fig. 4 c and d. Table 3 shows the estimated emission bandwidth (FWHM) around 1030 nm of various Ga concentration from 80 K to 300 K.

It can be observed that the bandwidth values at room temperature are relatively high (9.3–10.9 nm) and when cooled down (e.g., to 100 K), the bandwidth value considerably reduced: 1.27 nm in the case of Yb:YAG to 5.65 nm after the 50% Ga^{3+} substitution for Al^{3+}. The latter value is lower than that at 40% Ga substitution which is 6.11 nm. Increasing to 100% Ga concentration on the other hand reduces the bandwidth to 1.1 nm. The obtained results were comparable with one of our previous works with 40% Ga substitution which is 6.55 nm at 100 K [21]. Thus, an addition of more than 40% Ga substitution does not help in improving the bandwidth at cryogenic temperatures.

3.2. Yb:YSAG system

Fig. 5 a) shows the XRD patterns of the Yb:YSAG system with Sc concentration (Sc substitution of 0, 10%, 30% and 50%). And the corresponding chemical formula is reported in Table 2. The XRD patterns showed the presence of secondary phases apart from the garnet phase, as is visible by the peaks in the detailed diffractogram on the right side of Fig. 5 a:a small amount of an orthorhombic ($YAlO_3$) phase and of Sc_2O_3. A possible explanation is a change in temperatures under which intermediate phases are formed in the YSAG system. Moreover, at high concentrations, the preferential occupation of crystal sites by different ions can also play a role. It can also be observed that diffraction peaks shift towards lower diffraction angle with the increase of Sc content. This corresponds to the increase of lattice parameter, in line with the larger size of Sc^{3+} ions in comparison to Al^{3+} (see Table 1). We also retrieved the lattice parameters using the Rietveld refinement and it shows a linear increase (see Fig. 5 b) with increasing Sc content. The effect of Sc addition on the microstructure is different compared to Ga: the microstructure is highly porous and the presence of secondary phases is confirmed also by the SEM observations (see the dark grey areas in Fig. 5 c). Fig. 6 a shows the emission spectra of a 3 at.% Yb:YSAG system measured around 1030 nm at 100 K. From the figure, we can infer that the substitution of Sc helps in improving the bandwidth even at cryogenic temperatures but not as much as in the case of Ga. Fig. 6 b) shows the significant narrowing of emission spectra of 50% Sc substitution when the sample is cooled down from 300 K to 100 K. To estimate the variation of emission bandwidth by substitution of Sc, we fitted the gaussian function and the resulting FWHM for the Yb:YSAG system are shown in Fig. 6 c and d). Table 4 shows the estimated emission bandwidth (FWHM) around 1030 nm of various Sc concentration from 80 K to 300 K. The bandwidth values at room temperature were relatively high, however when cooled down they were considerably reduced. In the case of 50% Sc substitution the bandwidth is 2.51 nm, which is lower than that for 30% Sc substitution (2.55 nm). From the results it is clear that the addition of Sc does not significantly improve the bandwidth at cryogenic temperatures.

3.3. Effect on Yb:YSGAG system

Fig. 7 a) shows the XRD patterns of the Yb:YSGAG system with Sc and Ga concentration (substitution of 0, 5%, 15% and 25% each) and the

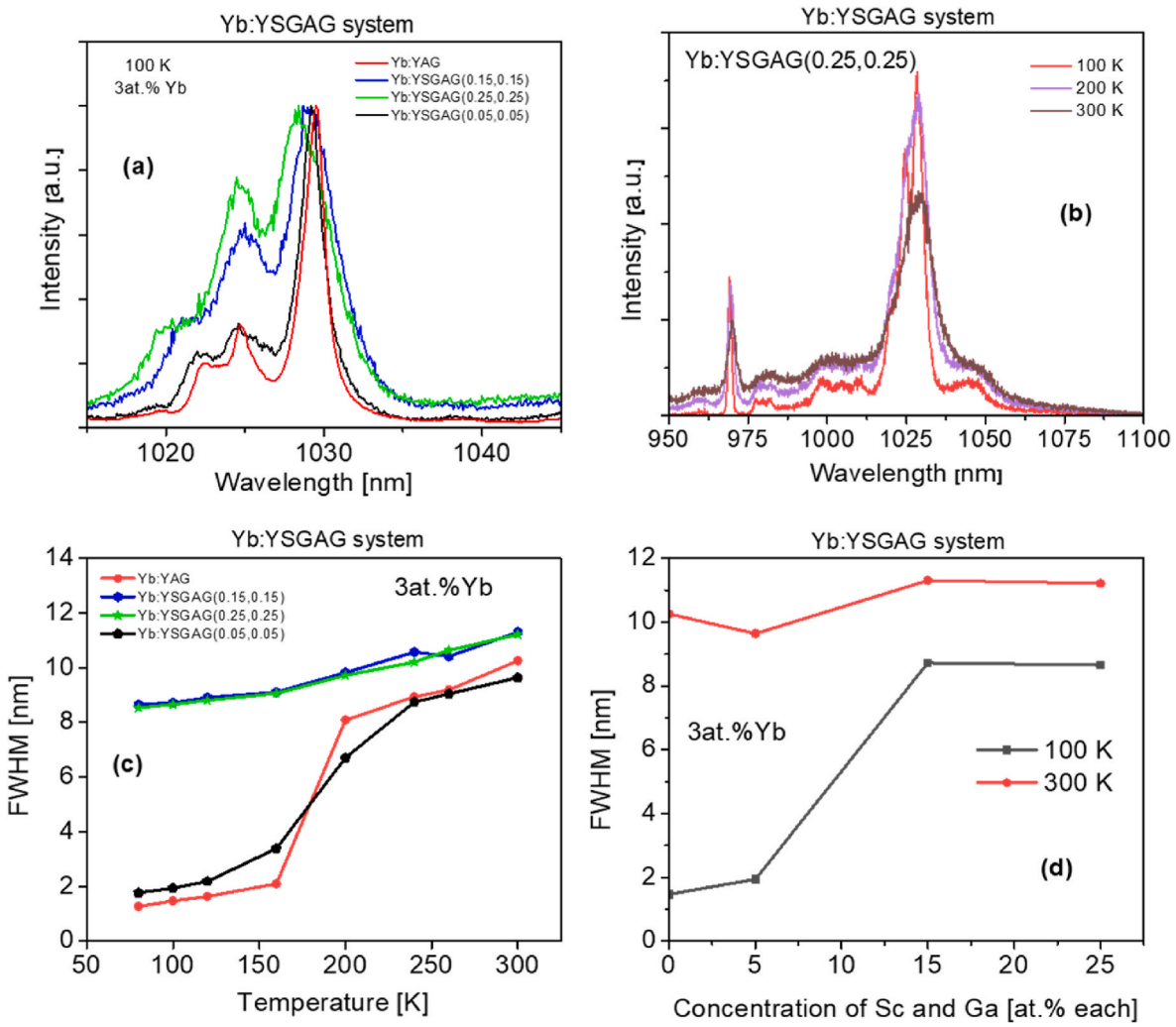

Fig. 8. Emission spectrum measured at 100 K for Yb:YSGAG system (a), emission spectra for sample with 25% Sc and 25% Ga for 100, 200 and 300 K (b), emission bandwidth (FWHM) at 1030 nm for various temperatures for Yb:YSGAG system (c), emission bandwidth (FWHM) at 1030 nm for different Sc and Ga content for 100 and 300 K (d).

Table 5
Emission bandwidth around 1030 nm for the Yb:YSGAG system for various temperatures.

	Emission bandwidth [nm] for the Yb:YSGAG system			
Temperature [K]	Yb: YAG	Yb:YSGAG (0.05,0.05)	Yb:YSGAG (0.15,0.15)	Yb:YSGAG (0.25,0.25)
80	1.27	1.77	8.65	8.54
100	1.47	1.94	8.72	8.66
120	1.63	2.19	8.91	8.81
160	2.10	3.39	9.11	9.06
200	8.09	6.71	9.82	9.72
240	8.94	8.75	10.57	10.21
260	9.19	9.05	10.42	10.64
300	10.26	9.64	11.31	11.22

corresponding chemical formula is reported in Table 2. The XRD patterns showed the presence of only the cubic garnet phase. As in the case of the other systems, the peaks shift towards lower diffraction angle with the increase of Sc and Ga content. This corresponds to the increase of the lattice parameter, in line with the larger size of Sc^{3+} and Ga^{3+} ions in comparison to Al^{3+} (see Table 1). The lattice parameters show a linear increase with increasing substitution (see 7 b). With respect to the ion size and coordination, the Sc^{3+} ions are much more likely to occupy the sixfold coordinated octahedral sites, while for Ga^{3+} ions there are no indications on preferential site occupation. With a higher level of mixed doping, the Ga^{3+} ions will thus be more likely to occupy the tetrahedral sites. The microstructure is less dense with larger voids in comparison to the other systems. No secondary phases were observed. The emission spectra of a 3 at.% Yb:YSGAG system measured around 1030 nm at 100 K (Fig. 8 a) show that the substitution of Sc and Ga leads to a higher increase of the bandwidth compared to the substitution with Ga or Sc alone. Fig. 8 b) shows the significant broadening of emission spectra of 25% Sc and Ga substitution when the sample is cooled down from 300 K to 100 K. Fig. 8 c and d) shows the estimated bandwidth (FWHM) of the Yb:YSGAG system around 1030 nm and the corresponding values are listed in Table 5. For example, at 100 K the bandwidth of Yb:YSGAG (0.15,0.15) is around 8.72 nm which is more than four times larger than that of the Yb:YAG system (1.94 nm). Theobtained results show that the addition of Sc and Ga together in the same system leads to a significant improvement of the bandwidth at cryogenic temperatures. Also, one can observe from the table of Yb:YSGAG (0.25,0.25) the bandwidth values slightly start reducing from that of Yb:SGAG (0.15,0.15). This might be due to the difference in occupancy factor of both Ga^{3+} and Sc^{3+} in the octahedral and tetragonal sites in the crystal lattice. Higher substitution of these cations will help to further determine the decrease in bandwidth.

4. Conclusions

In conclusion, we studied the effect of $Ga^{3+}$and Sc^{3+} on Yb:YAG emission at cryogenic temperatures on three mixed garnet systems, namely Yb:YGAG, Yb:YSAG and Yb:YSGAG. The samples were prepared by solid state sintering and were characterized in terms of structure and cryogenic emission. XRD studies were made and from the results the lattice parameters were retrieved using Rietveld method. All the three systems show a linear increase in lattice parameter that follows the introduction of larger ions of Ga^{3+} and Sc^{3+} in place of Al^{3+} in the YAG crystal. No significant effect on the sintering behaviour was observed, except for the fully substituted YGG system, which densified more compared to the other tested compositions. The cryogenic emission spectra of all the three systems were reported for different temperatures from room temperature down to 80 K and the Yb:YSGAG system provides promising results showing a significant emission broadening. Further work will be focused on optimizing the concentration of Ga and Sc content in YSGAG system and obtaining an optically transparent material for laser operation.

CRediT authorship contribution statement

Jan Hostaša: Writing – review & editing, Writing – original draft, Methodology, Investigation, Conceptualization. **Venkatesan Jambunathan:** Writing – review & editing, Writing – original draft, Methodology, Investigation, Funding acquisition, Conceptualization. **Dariia Chernomorets:** Writing – review & editing, Investigation. **Andreana Piancastelli:** Investigation. **Chiara Zanelli:** Investigation. **Great Chayran:** Investigation. **Francesco Picelli:** Investigation. **Martin Smrž:** Writing – review & editing, Resources. **Valentina Biasini:** Writing – review & editing, Supervision, Funding acquisition. **Tomáš Mocek:** Writing – review & editing, Supervision, Funding acquisition. **Laura Esposito:** Writing – review & editing, Supervision.

Declaration of competing interest

The authors declare the following financial interests/personal relationships which may be considered as potential competing interests:

Tomas Mocek reports financial support was provided by European Regional Development Fund and the state budget of the Czech Republic. Tomas Mocek reports was provided by European Commission. Valentina Biasini reports financial support was provided by National Research Council of Italy. Venkatesan Jambunathan reports financial support was provided by Czech Academy of Sciences. If there are other authors, they declare that they have no known competing financial interests or personal relationships that could have appeared to influence the work reported in this paper.

Data availability

Data will be made available on request.

Acknowledgements

This work was co-financed by the European Regional Development Fund and the state budget of the Czech Republic (project HiLASE CoE: Grant No. CZ.02.1.01/0.0/0.0/15_006/0000674) and by the EU's Horizon 2020 research and innovation programme under grant agreement No. 739573. The authors gratefully acknowledge the financial support for international cooperation by the Mobility Plus Program of the Czech Academy of Sciences (CNR-19-04) and by the bilateral program of the National Research Council of Italy (CNR/CAS 2019–2021).

References

[1] P. Ball, Laser fusion experiment extracts net energy from fuel, Nature (2014) 14710, https://doi.org/10.1038/nature.2014.14710 nature.2014.
[2] T. Haarlammert, H. Zacharias, Application of high harmonic radiation in surface science, Curr. Opin. Solid State Mater. Sci. 13 (2009) 13–27, https://doi.org/10.1016/j.cossms.2008.12.003.
[3] S. Kashiwagi, R. Kuroda, T. Oshima, F. Nagasawa, T. Kobuki, D. Ueyama, Y. Hama, M. Washio, K. Ushida, H. Hayano, J. Urakawa, Compact soft x-ray source using Thomson scattering, J. Appl. Phys. 98 (2005) 123302, https://doi.org/10.1063/1.2148619.
[4] A. Gujba, M. Medraj, Laser peening process and its impact on materials properties in comparison with shot peening and ultrasonic impact peening, Materials 7 (2014) 7925–7974, https://doi.org/10.3390/ma7127925.
[5] D. Brown, S. Tornegård, J. Kolis, C. McMillen, C. Moore, L. Sanjeewa, C. Hancock, The application of cryogenic laser physics to the development of high average power ultra-short pulse lasers, Appl. Sci. 6 (2016) 23, https://doi.org/10.3390/app6010023.
[6] D.C. Brown, S. Tornegård, J. Kolis, Cryogenic nanosecond and picosecond high average and peak power (HAPP) pump lasers for ultrafast applications, High Pow. Laser Sci. Eng. 4 (2016) e15, https://doi.org/10.1017/hpl.2016.12.
[7] S. Banerjee, P. Mason, J. Phillips, J. Smith, T. Butcher, J. Spear, M. De Vido, G. Quinn, D. Clarke, K. Ertel, C. Hernandez-Gomez, C. Edwards, J. Collier, Pushing the boundaries of diode-pumped solid-state lasers for high-energy applications, High Pow. Laser Sci. Eng. 8 (2020) e20, https://doi.org/10.1017/hpl.2020.20.
[8] V. Jambunathan, T. Miura, L. Těsnohlídková, A. Lucianetti, T. Mocek, Efficient laser performance of a cryogenic Yb:YAG laser pumped by fiber coupled 940 and 969 nm laser diodes, Laser Phys. Lett. 12 (2015) 015002, https://doi.org/10.1088/1612-2011/12/1/015002.
[9] V. Jambunathan, L. Horackova, P. Navratil, A. Lucianetti, T. Mocek, Cryogenic Yb:YAG laser pumped by VBG-stabilized narrowband laser diode at 969 nm, IEEE Photon. Technol. Lett. 28 (2016) 1328–1331, https://doi.org/10.1109/LPT.2016.2541218.
[10] V. Jambunathan, J. Koerner, P. Sikocinski, M. Divoky, M. Sawicka, A. Lucianetti, J. Hein, T. Mocek, Spectroscopic characterization of various Yb^{3+} doped laser materials at cryogenic temperatures for the development of high energy class diode pumped solid state lasers, Proc. SPIE 8780 (2013) 87800G, https://doi.org/10.1117/12.2016915.
[11] J. Körner, V. Jambunathan, J. Hein, R. Seifert, M. Loeser, M. Siebold, U. Schramm, P. Sikocinski, A. Lucianetti, T. Mocek, M.C. Kaluza, Spectroscopic characterization of Yb^{3+}-doped laser materials at cryogenic temperatures, Appl. Phys. B 116 (2014) 75–81, https://doi.org/10.1007/s00340-013-5650-8.
[12] G. Toci, A. Pirri, W. Ryba-Romanowski, M. Berkowski, M. Vannini, Spectroscopy and CW first laser operation of Yb-doped $Gd_3(Al_{0.5}Ga_{0.5})_5O_{12}$ crystal, Opt. Mater. Express 7 (2017) 170, https://doi.org/10.1364/OME.7.000170.
[13] G. Toci, A. Pirri, B. Patrizi, Y. Feng, T. Xie, Z. Yang, J. Li, M. Vannini, An in depth characterization of the spectroscopic properties and laser action of 10 at% Yb doped $_3Sc_xAl_{5-x}O_{12}$ (x = 0.25, 0.5, 1.0, 1.5) transparent ceramics, Ceram. Int. 46 (2020) 17252–17260, https://doi.org/10.1016/j.ceramint.2020.04.012.
[14] B.M. Walsh, N.P. Barnes, R.L. Hutcheson, R.W. Equall, B. Di Bartolo, Spectroscopy and lasing characteristics of Nd-doped $Y_3Ga_xAl_{(5-x)}O_{12}$ materials: application toward a compositionally tuned 094-μm laser, J. Opt. Soc. Am. B 15 (1998) 2794, https://doi.org/10.1364/JOSAB.15.002794.
[15] Y. Kuwano, K. Suda, N. Ishizawa, T. Yamada, Crystal growth and properties of $(Lu,Y)_3Al_5O_{12}$, J. Cryst. Growth 260 (2004) 159–165, https://doi.org/10.1016/j.jcrysgro.2003.08.060.
[16] G. Toci, A. Pirri, J. Li, T. Xie, Y. Pan, M. Nikl, V. Babin, A. Beitlerová, M. Vannini, First laser operation and spectroscopic characterization of mixed garnet Yb:LuYAG ceramics, Proc. SPIE 9726 (2016) 97261N, https://doi.org/10.1117/12.2209558.
[17] S. Slimi, V. Jambunathan, M. Pan, Y. Wang, W. Chen, P. Loiko, R.M. Solé, M. Aguiló, F. Díaz, M. Smrz, T. Mocek, X. Mateos, Cryogenic laser operation of a "mixed" Yb:LuYAG garnet crystal, Appl. Phys. B 129 (2023) 57, https://doi.org/10.1007/s00340-023-07999-9.
[18] Z. Fan, H. Liu, C. Wu, D. Xu, T. Ren, H. Li, Z. Sun, G. Jin, C. Xin, First-principles calculation and experimental study of mixed crystal $Tm:(Lu_xY_{1-x})_3AG$, Infrared Phys. Technol. 130 (2023) 104588, https://doi.org/10.1016/j.infrared.2023.104588.
[19] Y. Feng, G. Toci, A. Pirri, B. Patrizi, X. Chen, J. Wei, H. Pan, X. Zhang, X. Li, M. Vannini, J. Li, Influences of the Sc^{3+} content on the microstructure and optical properties of 10 at.% $Yb:Y_3Sc_xAl_{5-x}O_{12}$ laser ceramics, J. Alloys Compd. 815 (2020) 152637, https://doi.org/10.1016/j.jallcom.2019.152637.
[20] V. Jambunathan, L. Horackova, T. Miura, J. Sulc, H. Jelínková, A. Endo, A. Lucianetti, T. Mocek, Spectroscopic and lasing characteristics of Yb:YGAG ceramic at cryogenic temperatures, Opt. Mater. Express 5 (2015) 1289, https://doi.org/10.1364/OME.5.001289.
[21] S.P. David, V. Jambunathan, F. Yue, P. Navratil, M. Mika, A. Lucianetti, T. Mocek, Effect of Gd^{3+}/Ga^{3+} on Yb^{3+} emission in mixed YAG at cryogenic temperature, Ceram. Int. 45 (2019) 9418–9422, https://doi.org/10.1016/j.ceramint.2018.08.241.
[22] Y. Feng, Z. Liu, G. Toci, A. Pirri, B. Patrizi, M. Vannini, D. Hreniak, J. Li, Fabrication, microstructure, spectral properties, and laser performance of Yb: $Gd_xY_{3-x}Al_5O_{12}$ ceramics, J. Am. Ceram. Soc. (2024) 1–13, https://doi.org/10.1111/jace.19711.
[23] R.D. Shannon, Revised effective ionic radii and systematic studies of interatomic distances in halides and chalcogenides, Acta Crystallogr. A 32 (1976) 751–767, https://doi.org/10.1107/S0567739476001551.